Dovepress

🔓 Open Access Full Text Article

ORIGINAL RESEARCH

Costunolide Inhibits Chronic Kidney Disease Development by Attenuating IKKβ/NF-κB Pathway

Yang Zhao [1],* , Yi-Han Wang[2],*, Wei-Chao Tu[1], Da-Wei Wang[1], Mu-Jun Lu[3,4], Yuan Shao[1]

[1]Department of Urology, Ruijin Hospital, School of Medicine, Shanghai Jiao Tong University, Shanghai, Shanghai, 201800, People's Republic of China; [2]Department of Urology, Sixth People's Hospital South Campus Affiliated to Shanghai Jiao Tong University, Shanghai, People's Republic of China; [3]Department of Urology and Andrology, Renji Hospital, School of Medicine, Shanghai Jiao Tong University, Shanghai, People's Republic of China; [4]Shanghai Institute of Andrology, Shanghai, People's Republic of China

*These authors contributed equally to this work

Correspondence: Mu-Jun Lu; Yuan Shao, Email lumujun@163.com; shaoyuan10772@163.com

Background: Chronic kidney disease (CKD) is a significant worldwide health concern that leads to high mortality rates. The bioactive substance costunolide (CTD) has demonstrated several pharmacological effects and holds promise as a CKD treatment. This study aims to investigate the impact of CTD on CKD and delve into its mechanisms of action.
Methods: Unilateral ureteral obstruction (UUO) methods and renal fibrosis mice models were created. Various concentrations of CTD were injected into UUO mice models to investigate the therapeutic effects of CTD on renal fibrosis of mice. Then, renal morphology, pathological changes, and the expression of genes related to fibrosis, inflammation and ferroptosis were analysed. RNA sequencing was utilized to identify the main biological processes and pathways involved in renal injury. Finally, both overexpression and inhibition of IKKβ were studied to examine their respective effects on fibrosis and inflammation in both in vitro and in vivo models.
Results: CTD treatment was found to significantly alleviate fibrosis, inflammation and ferroptosis in UUO-induced renal fibrosis mice models. The results of RNA sequencing suggested that the IKKβ acted as key regulatory factor in renal injury and the expression of IKKβ was increased in vitro and in vivo renal fibrosis model. Functionally, down-regulated IKKβ expression inhibits ferroptosis, inflammatory cytokine production and collagen deposition. Conversely, IKKβ overexpression exacerbates progressive renal fibrosis. Mechanistically, CTD alleviated renal fibrosis and inflammation by inhibiting the expression of IKKβ and attenuating IKKβ/NF-κB pathway.
**Conclusion:** This study demonstrates that CTD could mitigate renal fibrosis, ferroptosis and inflammation in CKD by modulating the IKKβ/NF-κB pathway, which indicates targeting IKKβ has an enormous potential for treating CKD.
Keywords: chronic kidney disease, costunolide, renal fibrosis, IKKβ/NF-κB pathway

Introduction

Chronic kidney disease (CKD), characterized by permanent alterations in kidney structure and function resulting from a variety of underlying diseases, is an important public health problem and the morbidity rate is estimated to be 8%–16% worldwide.[1–3] Patients with CKD often suffer from cardiovascular disease, which results in high morbidity and mortality.[4] Renal fibrosis, which involves the excessive accumulation of extracellular matrix (ECM) proteins in the renal tubule interstitium and glomerulus, represents a common endpoint of CKD.[5,6] The pathogenesis of renal fibrosis can be categorized into four interconnected stages: priming, activation, execution, and progression.[7] In short, inflammatory cells are massively infiltrated into renal tubules after injury and contribute to the accumulation of ECM and renal tubular atrophy, all of which result in renal fibrosis and dysfunction.[8–10] The fundamental principle for treating CKD lies in stopping or retarding the progression of renal fibrosis. However, an approved treatment targeting to renal fibrosis is almost nonexistent.

Graphical Abstract
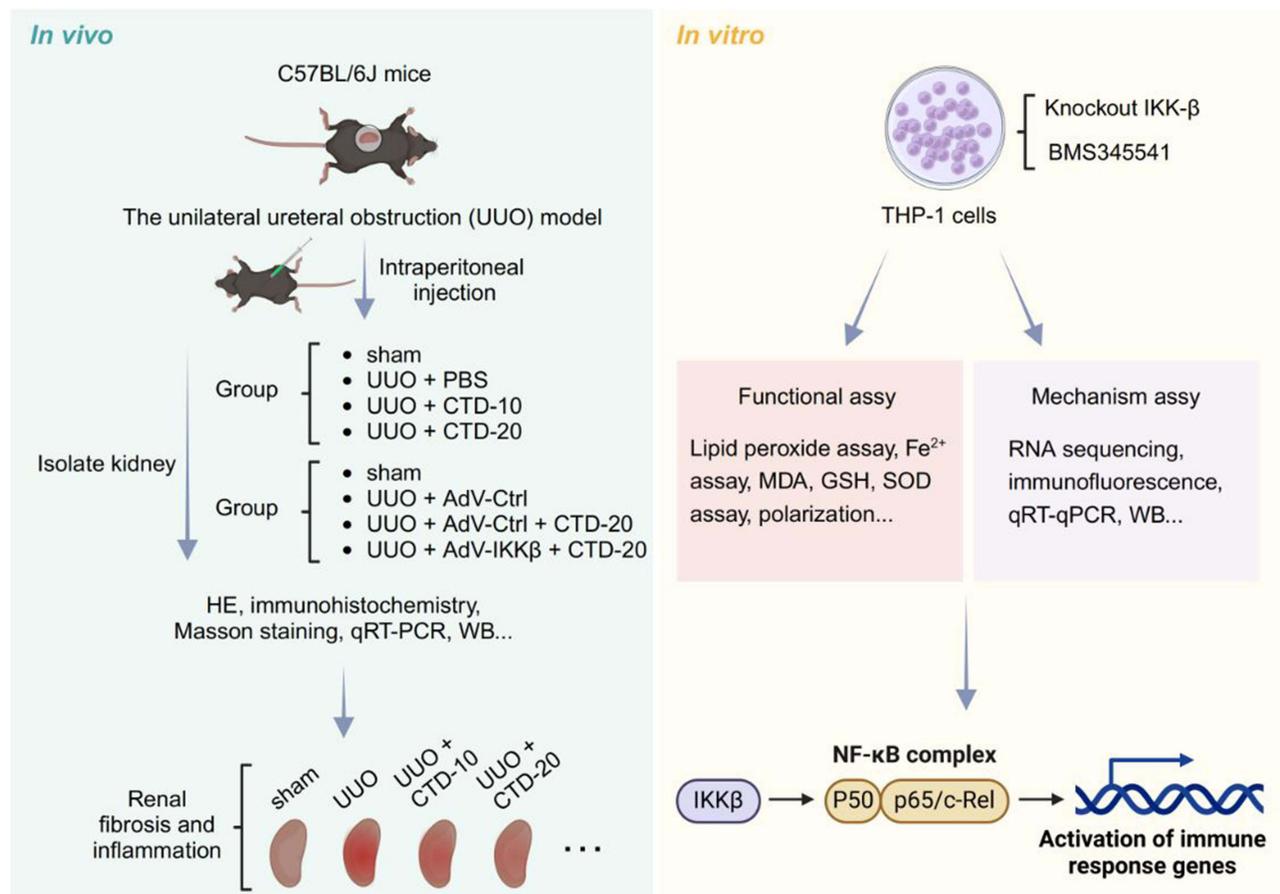
The development of CKD is also influenced by systemic inflammation. Nevertheless, the precise timeframe linking inflammation and CKD remains uncertain. Systemic inflammation is distinguished by the ongoing existence of inflammatory markers.[11] There is some evidence indicating that the IL-1β/IL-18 axis plays a role in the advancement of CKD. More specifically, the levels of IL-18 might have a connection to monocyte chemoattractant protein 1 (MCP-1), whereas MCP-1 is also linked to estimated glomerular filtration rate (eGFR) in an independent manner. Moreover, IL-18 is associated with the inflammation and calcification of blood vessels in individuals with CKD.[12] In CKD, macrophages can polarize into two different phenotypes: M1 (classical activation) and M2 (alternative activation).[13] M1 macrophages are mainly associated with proinflammatory responses, while M2 macrophages are associated with anti-inflammatory responses, tissue repair, and fibrosis.[14] During renal fibrosis, the increase in M1 macrophages is associated with the production of fibrotic factors and the deposition of extracellular matrix, which in turn promotes the progression of fibrosis.[15] In addition, macrophages can produce a large amount of reactive oxygen species (ROS) during polarization, leading to increased oxidative stress. These ROS can directly damage renal cells and promote the expression of inflammatory and fibrotic genes.[16]

In addition, the occurrence of ferroptosis is closely related to kidney damage. Ferroptosis is a type of iron-dependent, non-apoptotic cell death mode, characterized by the accumulation of ROS.[17] In terms of biochemistry, in the cellular aspect, glutathione (GSH) depletion and glutathione peroxidase 4 (GPX4) activity reduction result in the inability of lipid peroxides to undergo the reduction reaction catalyzed by GPX4. Fe^{2+} oxidizes lipids in a Fenton-like manner, generating

a large amount of ROS and promoting ferroptosis.[18] However, whether ferroptosis affects the occurrence and development of CKD and what the specific molecular mechanism is remains to be further explored.

Therapeutic agents sourced from nature, particularly from plants, have long been acknowledged as valuable products.[19] Costunolide (CTD) is a sesquiterpene lactone that can be isolated from various plants.[20] It has multiple properties, including anti-proliferative, anti-inflammatory, and anti-oxidative effect.[21] Reports suggested that CTD hindered the growth of colorectal cancer cells and triggered apoptosis in their corresponding cell lines.[22,23] Nuclear factor kappa B (NF-κB) signaling pathway is an important signaling factor that regulates gene transcription and controls various processes such as immunity, inflammation, cell growth, and apoptosis. An overactive NF-κB signaling pathway plays a key role in renal fibrosis.[24] Overactive NF-κB leads to the activation and recruitment of immune cells. In turn, inflammation triggers oxidative stress by activating leukocytes and resident cells to produce reactive oxygen and nitrogen species. Therefore, developing strategies to target the NF-κB signaling pathway is important for the effective treatment of renal fibrosis.[25] Several studies have suggested that the anti-inflammatory properties of CTD may be attributed to its ability to inhibit the NF-κB signaling pathway.[26,27] Despite its potential benefits, the impact of CTD on the advancement of renal fibrosis in CKD has yet to be determined.

In the present study, we hypothesized that CTD inhibits ferroptosis and reduces inflammation, thereby alleviating renal injury and fibrosis through the inhibition of the NF-κB signaling pathway. To achieve this, we established a mouse model of renal injury using UUO and studied the effects of CTD on the development of CKD.

Materials and Methods
Animals
Forty male C57BL/6J mice, aged 6–8 weeks and of specific pathogen-free grade, were provided with free access to food and water. Room temperature was maintained at 20–24°C and relative humidity at 40% to 60%. The mice were purchased from Weitong Lihua Company (Beijing, China).

The Unilateral Ureteral Obstruction (UUO) Model
The mice were randomly divided into four groups of five: sham-operated, UUO-PBS, UUO+CTD-10, and UUO+CTD-20. UUO surgical preparation was conducted following a previously described protocol.[28] In short, an opening was made 1cm to the left side of the spine above the thigh of the mouse, and the kidney was exposed by successively cutting the epidermis, mucosa, and muscle with surgical scissors. The kidney was carefully and gently squeezed out. The ureter was isolated at the upper 1/3 of the ureter. The ureter was ligated with silk thread at its proximal and distal ends, cut in between, and the kidney was gently placed using a cotton ball. The muscle and skin were sutured with needle and thread in turn. Iodine tincture was applied to the wound, and the mice were returned to the cage until they woke up. Following the ligation procedure, mice received intraperitoneal injections of CTD (10 mg/kg/day) or CTD (20 mg/kg/day) one day after. CTD was procured from Sigma (MO, USA). Those mice were injected with 1 μL adenovirus carrying (AdV)-ctrl and AdV-IKKβ via tail vein one day after UUO-treated at a titer of 5×10^8 TU (GenePharma, Shanghai, China).

At the 7-day mark following the UUO procedure, the mice were sacrificed. The kidneys were extracted, weighed, and measured for length. A portion of the left kidney was fixed in 10% neutral buffered formalin, embedded in paraffin, and used for pathology, histopathology, and immunohistochemistry analyses. The rest of the kidneys from each group were stored in liquid nitrogen for RT-qPCR and Western blot.

Hematoxylin-Eosin (HE) Staining and Periodic Acid-Schiff (PAS) Staining
HE staining was performed using the HE staining Kit (Solarbio, Beijing, China). HE staining was carried out on 4-μM-thick sections for 1 min, followed by differentiation in acidic alcohol for 30 seconds. The sections were then dehydrated in 95% ethanol for 50 seconds, cleared in xylene, and mounted. The changes of glycogen content in kidney tissue were detected by PAS staining kit (Beyotime, Shanghai, China). The kidney sections were hydrated with distilled water and incubated with periodic acid solution for 5 min, followed by Schiff's Solution for 15 min. The sections were

counterstained with hematoxylin solution for 1.5 min. The captured images were analyzed using the Image J software after being viewed under the Ci-L microscope (Nikon, Japan).

Immunohistochemistry (IHC)

Kidney tissues were embedded in paraffin, fixed and cut into 4-µM-thick sections for immunohistochemical staining. The sections treated with 3% H_2O_2 and blocked with serum. Then, the sections were incubated with primary antibodies 24 hours (hs) at 4 °C, followed by secondary antibodies. Slides were incubated with diaminobenzidine and nuclear was stained with hematoxylin. The captured images were analyzed using the Image J software after being viewed under the Ci-L microscope (Nikon, Japan).

Masson Staining

Masson staining was carried out using the Masson Stain Kit (Sigma, St. Louis, MO, USA), following the provided instructions. The extent of renal fibrosis was assessed by calculating the proportion of blue-colored regions (indicating collagen) or fibrotic renal tissue. To obtain measurements of fibrosis, more than 25 fields were assessed in each group.

Cell Culture

The THP-1 cell was obtained from Shanghai Zhongqiao Xinzhou Biotechnology in Shanghai, China. The cells were grown in RPMI-1640 (Thermo Fisher, Waltham, MA, USA) supplemented with 10% fetal bovine serum (Gibco, Rockville, MD, USA) and 100 U/mL penicillin mixture (Thermo Fisher, Waltham, MA, USA) at 37°C with 5% CO_2. For the IKKβ group, the THP-1 cells were exposed to IKKβ at a concentration of 5 µM for 24 hs. In the IKKβ+CTD group, the cells were exposed to CTD for an additional 24 hs at concentrations of either 5 µM or 10 µM.

Cell Transfection

The cells were inoculated on six-well plates at approximately 5×10^6 cells per well and stimulated with PMA (Sigma, St. Louis, MO, USA) for 48 hs. The medium was replaced with fresh medium supplemented with 20% FBS without antibiotics. The small interfering-control (sictrl), siRNA-IKKβ (si-IKKβ), AdV-ctrl and AdV-IKKβ (GenePharma, Shanghai, China) were prepared at a final concentration of 10 nM, following the manufacturer's instructions. Lipofectamine™ 2000 was used to transfect the corresponding plasmid into THP-1 cells for 12 hs. The H_2O_2 was then added to stimulate the cells.

RNA Extraction and RNA Sequencing

After drug treatment, THP-1 cell was collected from the Control, LPS, and LPS+CTD (10 µM) group. Total RNA from the sample was isolated using TRIzol reagent (Invitrogen, Waltham, MA, USA). RNA sequencing was performed by Wuhan Maiwei Metabolic Biotechnology (Wuhan, Hubei, China). Differential expression analysis was performed after obtaining raw data from RNA sequencing using R language (version 4.2.0). To identify significantly different genes, a threshold of $P \leq 0.05$ and a fold change of ≥ 2 were set. The Gene Ontology (GO) and Kyoto Encyclopedia of Genes and Genomes (KEGG) pathway were conducted using the "clusterProfiler" package in R software.

Immunofluorescence

The kidneys were fixed through perfusion with 4% paraformaldehyde (servicebio, Wuhan, Hubei, China). Tissue sections of 5 µM were deparaffinized in toluene and rehydrated using graded ethanol. Antigen retrieval was performed by microwave for 10 min. To block non-specific binding, the sections were incubated with 20% goat serum in PBS for 30 min. Monoclonal antibodies including anti-αSMA (Sigma, St. Louis, MO, USA) at a dilution of 1:100, anti-F4/80 (AbD Serotec, Oxford, UK) at a dilution of 1:200, anti-Ly-6G (AbD Serotec, Oxford, UK) at a dilution of 1:200, and anti-CD3 (Sigma, St. Louis, MO, USA) at a dilution of 1:100 was incubated with the sections overnight at 4°C. The sections were then exposed to Alexa 594-conjugated secondary anti-mouse IgG antibodies (Invitrogen, Carlsbad, CA, USA) at a dilution of 1:500 for 1 h. Nuclear staining was performed using DAPI, and the sections were imaged using a Leica

Table 1 Primer Sequence

Gene	Forward (5'→3')	Reverse (5'→3')
Vim	CGTCCACACGCACCTACAG	GGGGGATGAGGAATAGAGGCT
Cola1	GCTCCTCTTAGGGGCCACT	CCACGTCTCACCATTGGGG
TNFβ1	CTCCCGTGGCTTCTAGTGC	GCCTTAGTTTGGACAGGATCTG
MMP2	CAAGTTCCCCGGCGATGTC	TTCTGGTCAAGGTCACCTGTC
TNF-α	CCTGTAGCCCACGTCGTAG	GGGAGTAGACAAGGTACAACCC
IL-6	CTGCAAGAGACTTCCATCCAG	AGTGGTATAGACAGGTCTGTTGG
IL-1β	GAAATGCCACCTTTTGACAGTG	TGGATGCTCTCATCAGGACAG
GADPH	TGCACCACCAACTGCTTAGC	GGCATGGACTGTGGTCATGAG

TCS SP5 confocal system (Leica Microsystems, Heidelberg, Germany). Immunofluorescence staining of cells was performed similarly to kidney tissue staining.

Real-Time Quantitative PCR (RT-qPCR)

Total RNA was extracted from the kidney using TRIzol reagent (Invitrogen, Waltham, MA, USA) and reversed transcribed into cDNA using a kit from Tiangen Biotechnology (Beijing, China). The PCR reaction was performed with 2x SYBR Green QPCR Master Mix (Shanghai Dongsheng Biotechnology, Shanghai, China), using GADPH as an internal control. The relative gene expression was determined by the $2^{-\Delta\Delta Ct}$ method, and the primer sequences used are provided in Table 1.

Western Blot

Protein extraction was performed using RIPA buffer (Shanghai Life Mode Engineering, Shanghai, China) supplemented with PMSF (Shanghai Life Mode Engineering, Shanghai, China). The protein concentration was determined using a BCA kit (Shanghai Dongsheng Biotechnology, Shanghai, China). The primary antibody (Table 2) was incubated with a PVDF membrane (0.22 μM, Millipore ISEQ00010, USA) at 4°C overnight, followed by incubation with a secondary antibody (1:2000, Abcam, Waltham, MA, USA) conjugated to HRP. Protein bands were visualized using Prime Western

Table 2 All Antibodies in This Study

Gene	Brand	Dilution Ratio	Provenance
αSMA	Abcam	1:1000	rabbit
Collagen I	Abcam	1:1000	rabbit
Fibronectin	Abcam	1:1000	rabbit
IL-1β	Abcam	1:1000	rabbit
TNF-α	Abcam	1:1000	rabbit
iNos	Abcam	1:1000	rabbit
GPX4	Abcam	1:1000	rabbit
ACSL4	Abcam	1:1000	rabbit
SLC7A11	Abcam	1:1000	rabbit
p65	Abcam	1:1000	rabbit
IKBα	Abcam	1:1000	rabbit
p-IKKβ	Abcam	1:1000	rabbit
p-ikkα	Abcam	1:1000	rabbit
IKKβ	Abcam	1:1000	rabbit
p-TAK1	Abcam	1:1000	rabbit
TAK1	Abcam	1:1000	rabbit
GADPH	Sigma	1:5000	mouse

Blotting Detection Reagent (Cytiva, UK), and the chemiluminescence was detected using a ChemiDoc MP imaging system (Tanon 4800, Shanghai, China). The gray value of the bands was analyzed using Image J software.

Lipid Peroxide Assay and Fe^{2+} Assay

The lipid peroxide was assayed by C11-BODIPY 581/591 lipid peroxidation sensor (Mao Kang, Shanghai, China). After treating the cells, they were incubated with C11-BODIPY 581/591 (10 μM) in a 24-well culture plate at 37°C for 1 h. After incubation, the cells were harvested and washed with PBS, then resuspended in 500 μL of PBS. The images were collected using IX83 fluorescence microscope (ECLIPSE Ts2R-FL, Nikon). For Fe^{2+} assay, according to the manufacturer's instructions, use the FerroOrange (Fe^{2+} indicator) (Mao kang, Shanghai, China) to measure the level of Fe^{2+} in cell. In short, Fe^{2+} reacts with the color reagent at 45°C for 60 min, generating a stable chromophore with a maximum absorption peak at 572 nm. The images were collected using IX83 fluorescence microscope (ECLIPSE Ts2R-FL, Nikon).

Intracellular Malondialdehyde (MDA), Glutathione (GSH) and Superoxide Dismutase (SOD) Assay

Cells were seeded overnight and treated with IKKβ and CTD for 24 hs. Then, the level of GSH was measured using MDA, GSH and SOD detection kit (Elabscience, Wuhan, China). In short, after 24 hs of treatment, cells were collected and protein extraction was performed using RIPA buffer (Shanghai Life Mode Engineering, Shanghai, China) supplemented with PMSF (Shanghai Life Mode Engineering, Shanghai, China). The protein concentration was determined using a BCA kit (Shanghai Dongsheng Biotechnology, Shanghai, China), and finally, measured using an enzyme immunoassay according to the manufacturer's instructions.

Statistical Analysis

All the experiments were presented as mean ± standard error of the mean (SEM, n ≥ 5). Using the SPSS 22.0 software performed statistical analysis and difference comparison on the experimental data. The one-way ANOVA analysis of variance was used to assess whether there were statistical differences between groups. A P-value of less than 0.05 was considered statistically significant.

Results
CTD Attenuates UUO-Induced Kidney Injury

After construction of UUO model, the kidneys of mice were extracted for further analysis. The pictures of the kidney are illustrated in Figure 1A. In comparison to the sham group, UUO treatment led to an increase in kidney length, kidney weight, and the ratio of kidney weight to contralateral non-obstructed kidney. However, administration of CTD resulted in a significant attenuation of these effects in UUO-treated kidneys (Figure 1B-D). After administration of CTD, the intratubular space and ECM deposition were reduced in UUO-treated kidneys compared to PBS group by HE and PAS staining (Figure 1E). Tubular injury score was increased after UUO, but CTD markedly prevented the tubular injury in UUO-treated kidneys (Supplementary Figure 1).

CTD Alleviates Renal Fibrosis Induced by UUO

Compared with the sham group, UUO-treated significantly increased renal fibrosis, but this fibrotic progression was attenuated after CTD administration (Figure 2A). The expression of αSMA was significantly increased in the UUO-treated group, while that in CTD treatment group was significantly decreased (Figure 2B). The expression of αSMA, Collagen I and Fibronectin was increased in UUO-treated kidneys, but CTD treatment significantly attenuated this increase when compared to PBS treatment in UUO-treated group (Figure 2C-D). We also detected elevated mRNA levels of Vim, Col1a1, Tgfb1, and Mmp2 in UUO-treated kidneys, and CTD reversed the UUO-induced mRNA change (Figure 2E-H).
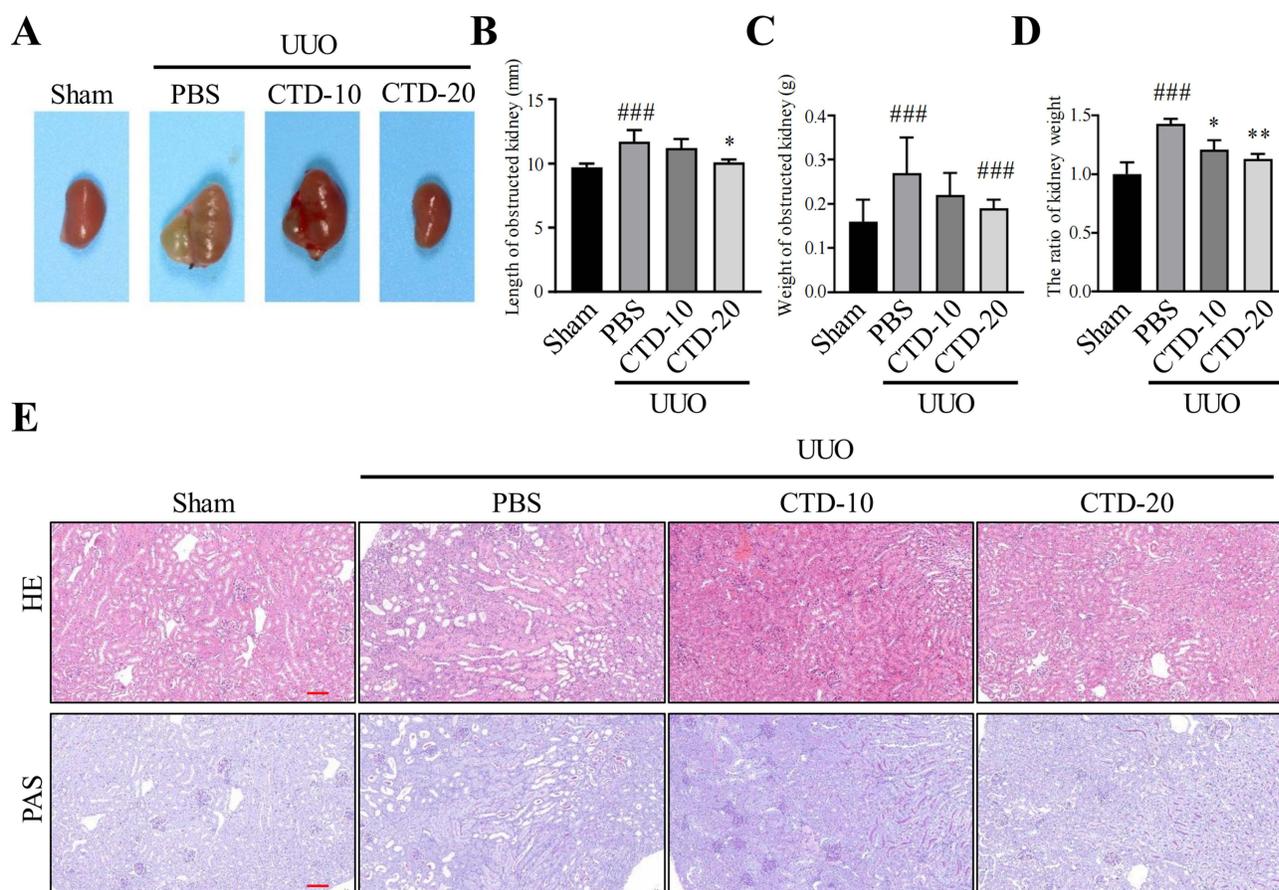
Figure 1 Effects of CTD on kidney of UUO-treated mice. (**A**) Representative pictures of kidney of mice after experiment, (**B**) kidney length, (**C**) kidney weight, (**D**) the ratio of kidney weight to contralateral non-obstructed kidney weight of experimental mice, (**E**) HE and PAS of histological structure of kidney in different groups, Scale bar: 100 μm; *$P < 0.05$, **$P < 0.01$, ####$P < 0.001$, compared to the UUO group, (n = 5 mice per group).

CTD Reduced Renal Inflammation and Ferroptosis Caused by UUO in vivo

In the UUO model, the kidney damage exacerbated due to renal inflammation, and our next objective is to assess the potential of CTD in suppressing UUO-induced inflammation. Compared to the sham group, the staining of F4/80, Ly-6G and CD3 were markedly increased in UUO group, while CTD treatment notably reduced these staining patterns (Supplementary Figure 2). Additionally, in the UUO group, the staining of F4/80 was significantly increased, but the expression of IL-1β was notably reduced with IL-1β treatment (Figure 3A). The mRNA levels of TNF-α, IL-6, and IL-1β were increased in UUO-treated kidneys according to RT-qPCR analysis, but CTD treatment led to a notable decrease in the expression of these genes (Figure 3B-3D). Additionally, in UUO-group, the level of oxidative stress was up-regulated in kidney by ROS staining; however, CTD treatment obviously restrains the oxidative stress induced by UUO (Figure 3E). Research has shown that the enhancement of oxidative stress has been confirmed as a key factor causing ferroptosis. Therefore, in order to evaluate the sensitivity of ferroptosis in the UUO kidney injury model to CTD, we measured the expression levels of key genes ACSL4, GPX4, and SLC7A11 associated with ferroptosis and confirmed the decrease of ACSL4 as well as the increase in GPX4 and SLC7A11 protein expression in the UUO+CTD group through IHC staining (Figure 3F).

CTD Inhibited the Activation of IKKβ/NF-κB Pathway in UUO-Induced Kidney Injury

To further explore the molecular mechanisms of CTD attenuating kidney injury, we performed RNA sequencing. The results showed that 551 genes were identified as up-regulated between UUO and sham group (n = 5), and 638 genes were identified as down-regulated between UUO+CTD and UUO group (n = 5), with 381 overlapping genes (Figure 4A).
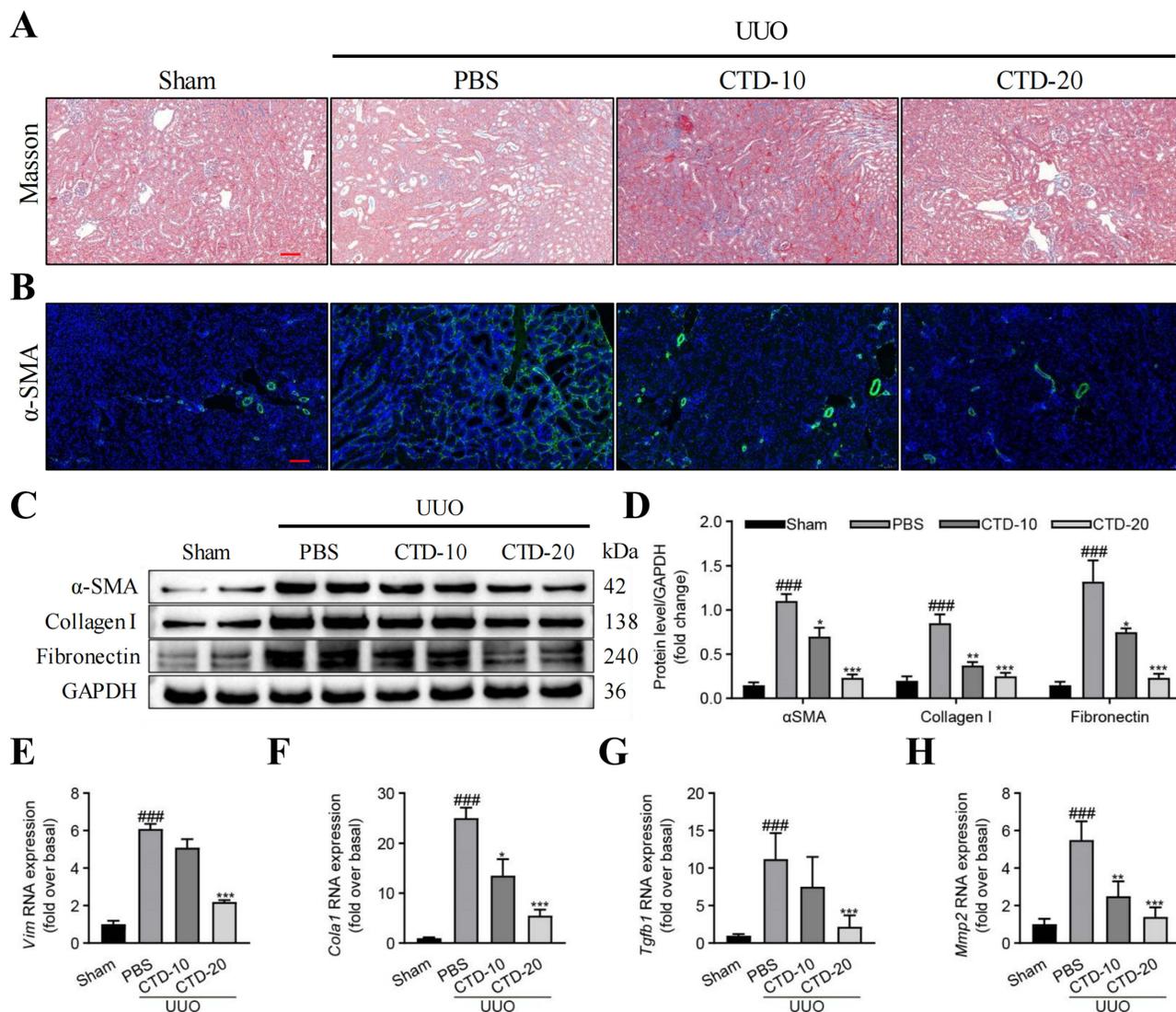
Figure 2 CTD suppresses renal fibrosis in UUO-induced kidney injury. (**A**) Masson staining of kidneys in each group (×200 magnification), Scale bar: 100 μm, (**B**) immunofluorescence staining of αSMA expression in kidneys, Scale bar: 100 μm, (**C**) Western blot analysis of αSMA, Collagen I, and Fibronectin expression, (**D**) quantification of Western blot results, qPCR analysis of mRNA expression of (**E**) Vim, (**F**) Cola1, (**G**) Tgfb1, (**H**) and Mmp2 in each group. [###] $P < 0.001$, compared to the sham group; *$P < 0.05$, **$P < 0.01$, ***$P < 0.001$, compared to the UUO group, (n = 5 mice per group).

KEGG analysis suggested that these 381 genes were mainly involved in the NF-κB signaling pathway (Figure 4B). The heatmap of NF-κB signaling pathway-related gene is shown in Figure 4C. The results of PPI network revealed that IKKβ was the most key hub gene among differential genes of NF-κB signaling (Figure 4D). IKKβ can activate NF-κB pathway and lead to macrophage polarization toward the M1 phenotype. The immunofluorescence results revealed that CTD reduced p-p65 and F4/80 activation in UUO-treated kidney (Figure 4E).

CTD Suppresses IKKβ-Induced Inflammation and Ferroptosis in vitro

We introduced IKKβ (Abcom, Germany) into THP-1 cells to examine whether CTD alleviates IKKβ-induced inflammatory response. According to RT-qPCR analysis, the expression of TNF-α and IL-6 was increased in the IKKβ-treated, which was prevented by CTD treatment (Figure 5A-B). Undoubtedly, the levels of TNF-α and IL-6 were decreased in the medium by CTD treatment (Figure 5C-D). The expression of Ptgs2, Ccl2, Nos2, and Nsfl1c was increased after IKKβ treatment, whereas treatment with different concentrations of CTD blocked this expression by RT-qPCR analysis (Supplementary Figure 3A–D). Compared to the control group, the expression
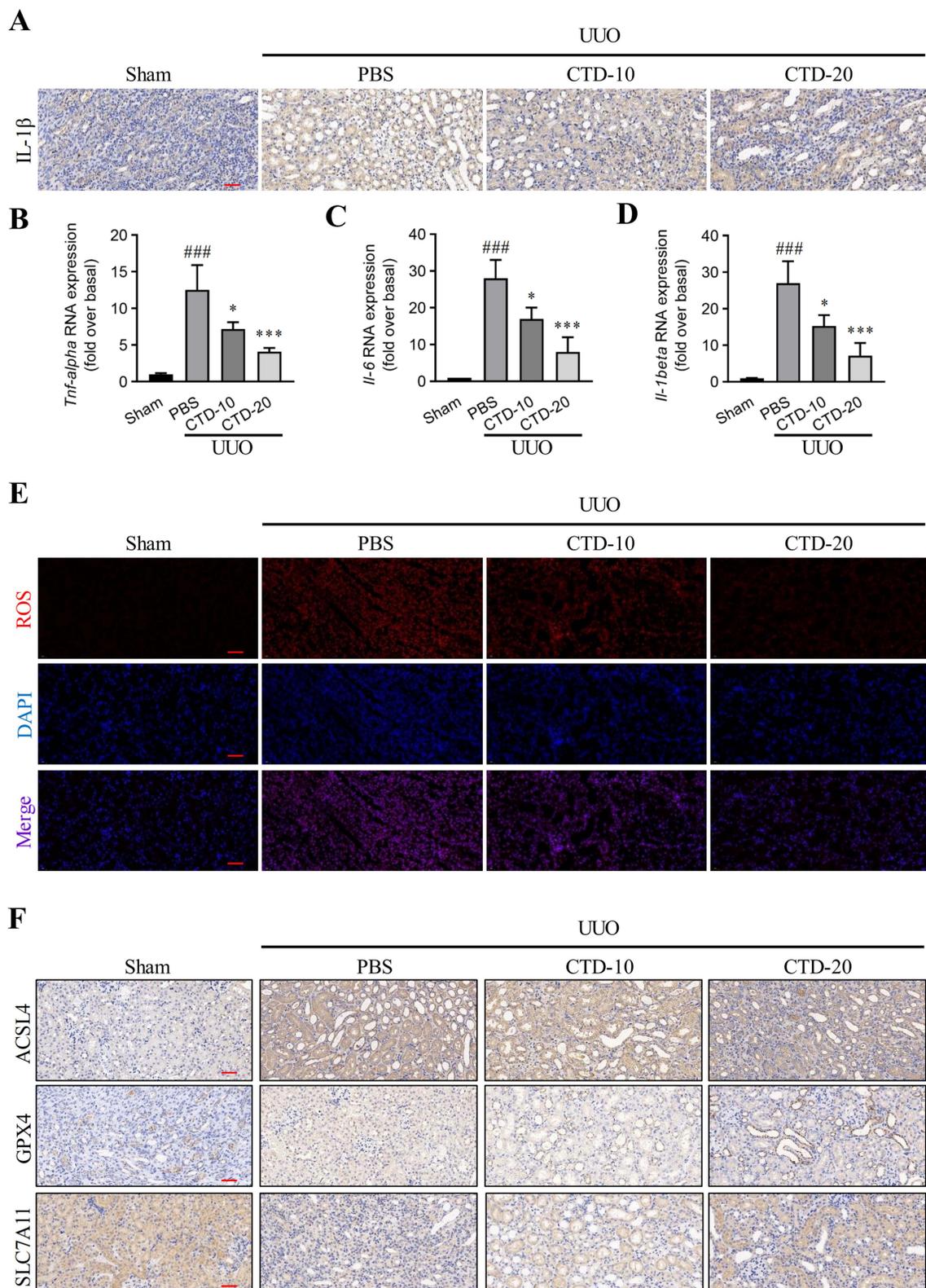
Figure 3 CTD inhibits UUO-induced inflammation and ferroptosis. (**A**) Representative pictures of IL-1β staining in each group, Scale bar: 100 μm, quantitative analysis of mRNA expression of (**B**) TNF-α, (**C**) Il-6, (**D**) and Il-1β in each group, (**E**) Representative pictures of ROS staining in each group, (**F**) Representative pictures of ACSL4, GPX4 and SLC7A11 staining in each group, Scale bar: 100 μm. $^{\#\#\#} P < 0.001$, compared to the sham group; $^{*}P < 0.05$, $^{***}P < 0.001$, compared to the UUO group, (n = 5 mice each group).
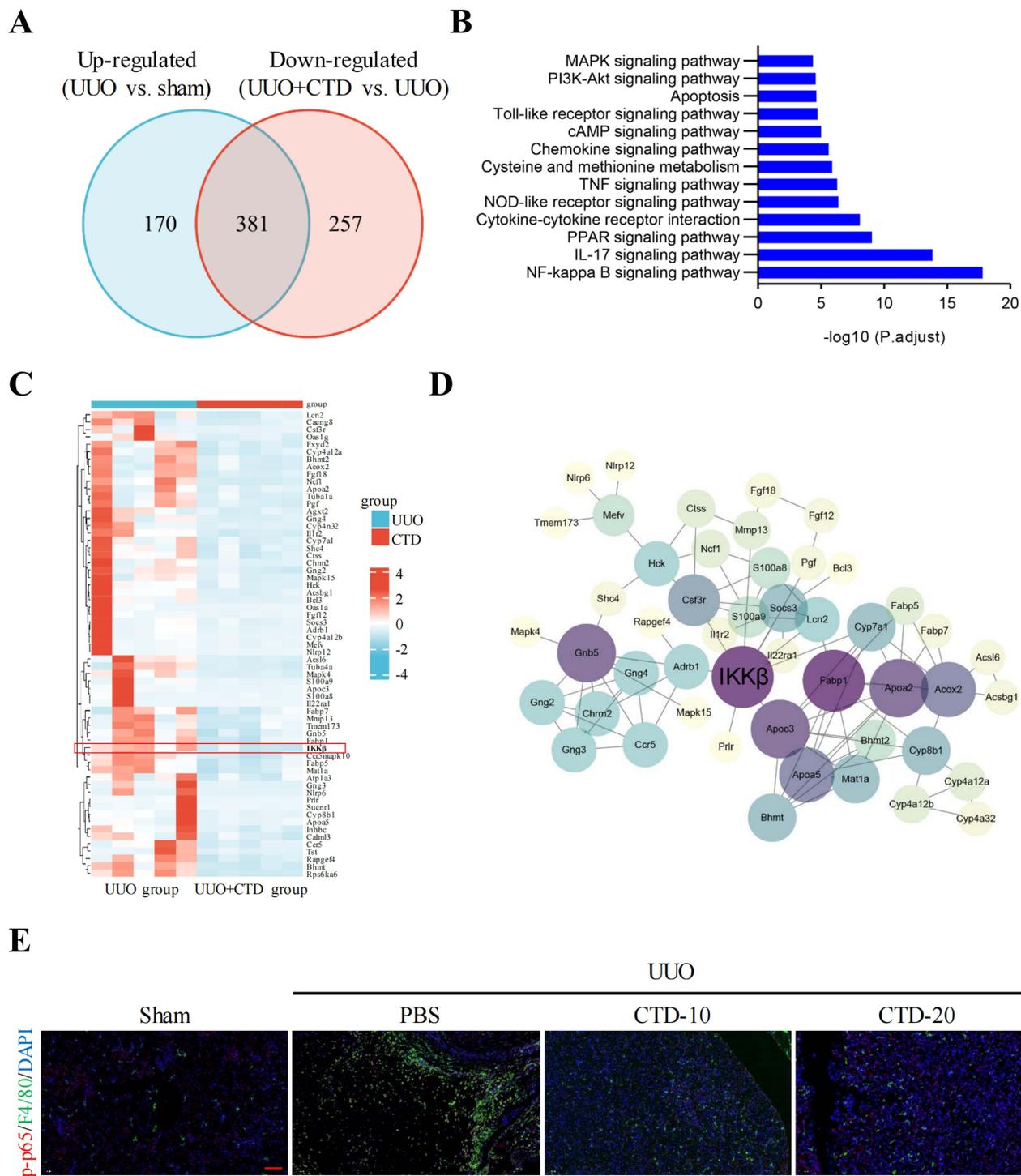
Figure 4 The protective effect of CTD against UUO-induced renal fibrosis may through the IKKβ/NF-κB pathway. (**A**) Intersection genes between the up-regulated genes in UUO vs sham group and the down-regulated genes in UUO+CKD vs UUO group, (**B**) KEGG enrichment analyses of intersection genes, (**C**) the heatmap of genes related to the NF-κB pathway, (**D**) PPI network of genes related to the NF-κB pathway, (**E**) immunofluorescence staining of p-p65 and F4/80, Scale bar: 100 μm, (n = 5 mice each group).

of iNOS was increased and CD206 was decreased in the IKKβ-treated, but CTD treatment led to the reversal of iNOS and CD206 expression (Figure 5E). Western blot analysis showed that IKKβ-treated increased the expression of TNF-α, IL-1β, and iNOS, but these expressions were decreased after CTD treatment (Supplementary Figure 4A–B). After CTD treatment, the expression of ACSL was inhibited compared with the
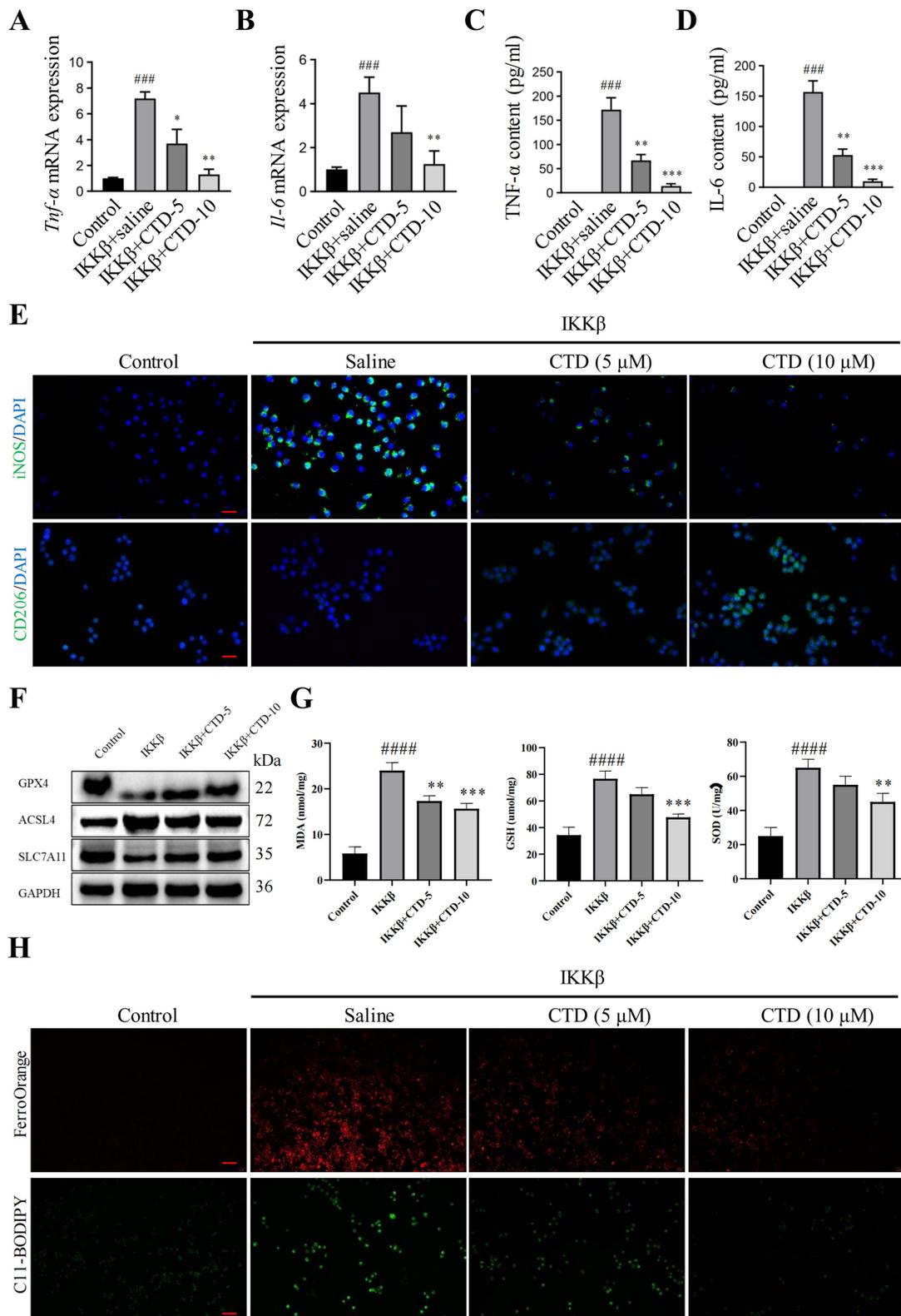
Figure 5 CTD suppresses IKKβ-induced inflammatory response in vitro. Quantitative analysis of mRNA expression of (**A**) *TNF-α*, and (**B**) *IL-6* in each group, the contents of (**C**) *TNF-α*, and (**D**) *IL-6* in the medium by ELISA assay, (**E**) immunofluorescence staining of iNOS and CD206 in each group from THP-1 cell, Scale bar: 50 μm, (**F**) the expression of ACSL4, GPX4 and SLC7A11 in each group, (**G**) ELISA detects the expression levels of lipid peroxidation markers MDA, GSH, and SOD in each group. (**H**) Representative pictures of Fe^{2+} and intracellular lipid peroxide in each group from THP-1 cells, Scale bar: 50 μm. ### $P < 0.001$, #### $P < 0.0001$, compared to the control group; *$P < 0.05$, **$P < 0.01$, ***$P < 0.001$, compared to the IKKβ+saline group, (n = 6 per group).

IKKβ group. Meanwhile, the decreased GPX4 and SLC7A11 expression in the IKKβ group was also reversed by CTD treatment (Figure 5F). MDA, GSH, and SOD measurements indicate that the lipid peroxidation levels of the IKKβ group were higher than the control group, while the addition of CTD can significantly reduce the level of lipid peroxidation (Figure 5G). The results of immunofluorescence also show that CTD can significantly inhibit the increase in Fe^{2+} content and lipid peroxidation levels induced by IKKβ (Figure 5H). Together, those results indicated that CTD suppresses IKKβ-induced inflammatory response and ferroptosis in THP-1 cell.

CTD Attenuates Inflammation by Inhibiting IKKβ Activation in vitro

In order to explore the role of IKKβ in inflammatory response, we have established IKKβ knockout in THP-1 cell (Figure 6A). Knockout IKKβ or addition of BMS345541 (the inhibitor of IKKβ) can obviously reduce the up-regulated expression of IL-1β induced by H_2O_2 (Figure 6B). In addition, the phosphorylation level of p65 was significantly reduced in the IKKβ knockout THP-1 cells and addition of BMS345541 in THP-1 cell (Figure 6C). Furthermore, H_2O_2 facilitates the expression of iNOS and restrains the expression of CD206. However, our results showed that knockout IKKβ or addition of BMS345541 can suppress the expression of iNOS and promote the expression of CD206 (Figure 6D). Together, those results showed that inhibition of IKKβ can significantly decrease the inflammatory response induced by H_2O_2 and promote M2 macrophage polarization in THP-1 cell.
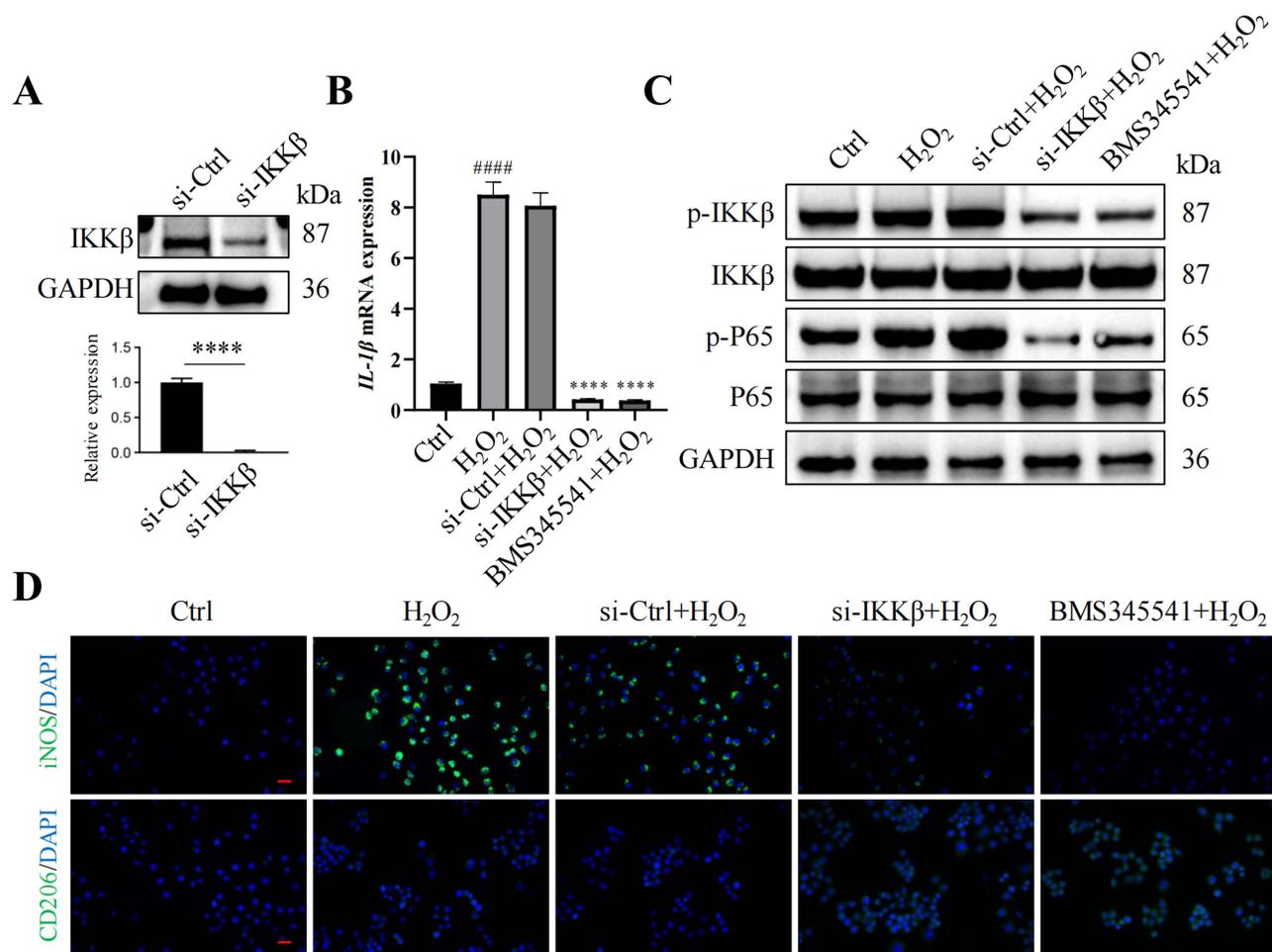
Figure 6 Inhibition of IKKβ can reduce the inflammatory response induced by H_2O_2. (**A**) Western blot analysis of IKKβ, (**B**) RT-qPCR analysis the expression of IL-1β in different groups after H_2O_2-treated, #### $P < 0.0001$, compared to the Ctrl group; ****$P < 0.0001$, compared to the siCtrl-H_2O_2 group. (**C**) Western blot analysis of p-IKKβ, IKKβ, p-P65 and P65 after H_2O_2-treated, (**D**) immunofluorescence staining of iNOS and CD206 in THP-1 cell, Scale bar: 100 μm, (n = 6 per group).
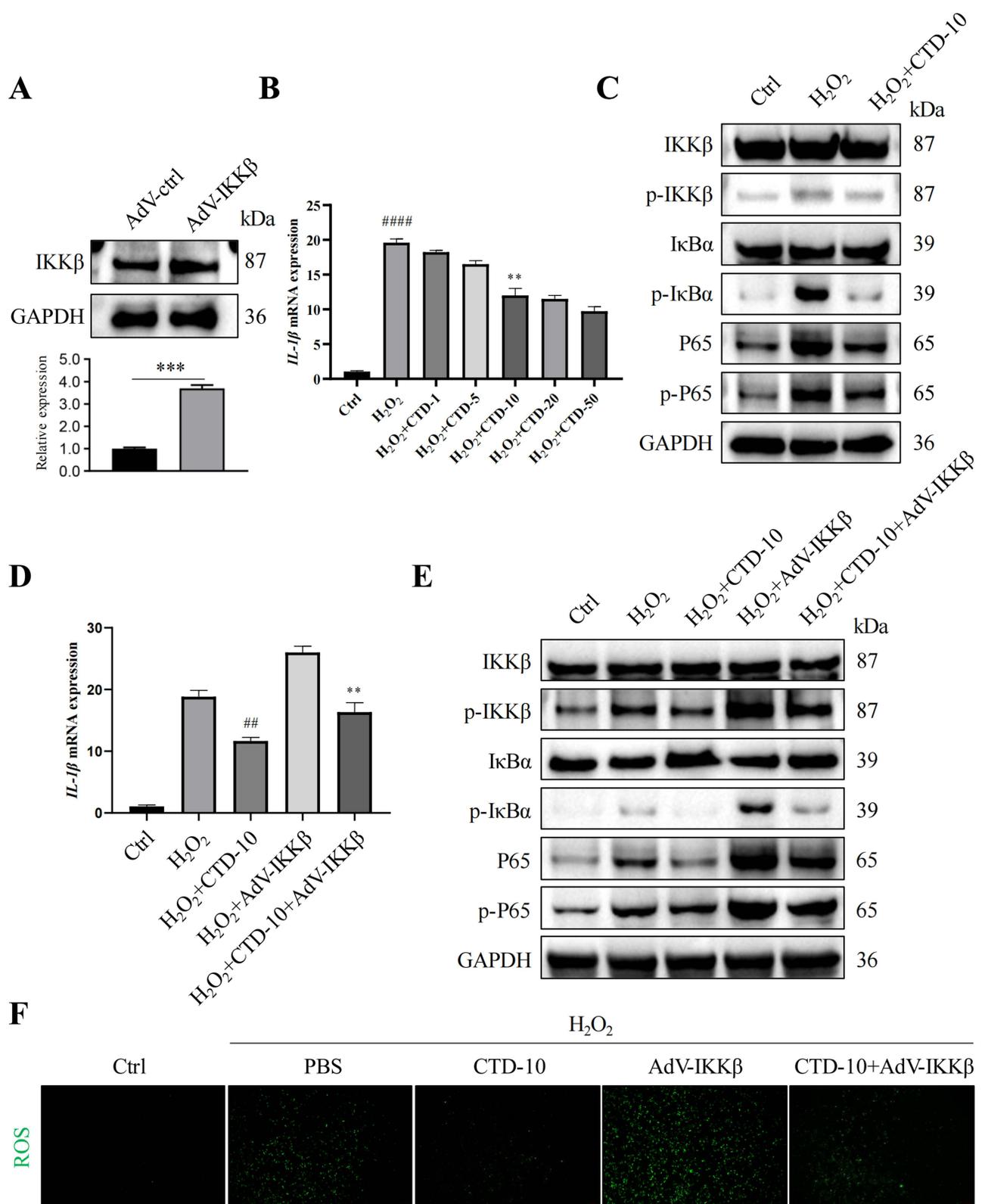
Figure 7 CTD were significantly weakened inflammatory response in vitro upon IKKβ overexpression. (**A**) The expression of IKKβ was detected by Western blot, (**B**) RT-qPCR analysis the expression of IL-1β in different CTD-treated group, $^{####} P < 0.0001$, compared to the Ctrl group; $^{**} P < 0.001$, compared to the H_2O_2 group. (**C**) Western blot analysis of p-IKKβ, IKKβ, IκBα, p-IκBα, p-P65 and P65 in different groups, (**D**) RT-qPCR analysis the expression of IL-1β in different group, $^{##} P < 0.01$, compared to the H_2O_2 group, $^{**}P < 0.01$, compared to the H_2O_2+AdV-IKKβ group. (**E**) Western blot analysis of p-IKKβ, IKKβ, IκBα, p-IκBα, p-P65 and P65 in different groups, (**F**) representative pictures of ROS staining in THP-1 cells, Scale bar: 50 μm, (n = 6 per group).

Next, we overexpressed IKKβ in the THP-1 cell (Figure 7A). Through RT-qPCR analysis, we found that CTD (10 μM) can reduce the increase of IL-1β mRNA level induced by H_2O_2 (Figure 7B). The results also showed that CTD (10 μM) can relieve the H_2O_2-induced increase of p-IKKβ, p-κBα and p-P65 expression (Figure 7C). Furthermore, CTD reduces the increase of IL-1β mRNA level induced by IKKβ (Figure 7D). Compared to AdV-IKKβ group, CTD reduced phosphorylation of IKKβ, leading to ubiquitination of IκB, resulting in reducing phosphorylation of p65 (Figure 7E). Additionally, AdV-IKKβ can exacerbate H_2O_2-induced oxidative stress in THP-1 cells; however, CTD can significantly inhibit this phenomenon (Figure 7F).

## CTD Attenuates Renal Injury by Inhibiting IKKβ Activation

The pictures of the kidney are illustrated in Figure 8A. Compared with AdV-Ctrl+CTD-20 group, kidney length, kidney weight, and the ratio of kidney weight to contralateral non-obstructed kidney weight were significantly increased in AdV-Ctrl and AdV-IKKβ+CTD-20 groups after UUO-treated (Figure 8B-D). Images of UUO+AdV-ctrl+CTD-20 and UUO+AdV-IKKβ+CTD-20 kidneys stained with PAS and Masson showed that UUO kidneys that were treated with CTD exhibited low intratubular space and higher ECM deposition (Figure 8E). Tubular injury score was decreased in the UUO+AdV-ctrl+CTD-20 group in contrast to the UUO+AdV-ctrl and UUO +AdV-IKKβ+CTD-20 group (Figure 8F). The expression of p-IKKβ, IKKβ, IκBα, p-IκBα, p-P65 and P65 was significantly decreased in UUO+AdV-ctrl+CTD-20 and UUO+AdV-IKKβ+CTD-20 versus to UUO+AdV-IKKβ group (Figure 8G). Based on immunofluorescence and IHC, the expression of F4/80 and IL-1β was decreased in the UUO+AdV-ctrl+CTD-20 group compared with the UUO+AdV-ctrl group, but overexpression of IKKβ alleviated F4/80 and IL-1β expression reduction (Figure 8H). Next, the levels of oxidative stress and iNOS were also restrained in the UUO+AdV-ctrl+CTD-20 group compared with the UUO+AdV-ctrl group; however, overexpression of IKKβ increased the levels of oxidative stress and iNOS versus to UUO+AdV-ctrl+CTD-20 group (Figure 8I). On the contrary, overexpression of IKKβ decreased the levels of CD206 versus to UUO+AdV-ctrl+CTD-20 group. All in all, CTD can attenuate renal injury induced by UUO-treated; however, overexpression of IKKβ partially alleviated the function of CTD.

Discussion

Chronic kidney disease (CKD) is a worldwide health concern with high morbidity and mortality rates, which ultimately leads to impaired kidney function due to renal fibrosis.[29] UUO has been shown to contribute to changes in renal hemodynamics and promote activation and proliferation of renal interstitial fibroblasts, eventually leading to tubular cell injury and renal dysfunction.[30,31] In this study, we found that UUO increased kidney length and weight. UUO also constituted severe tubular atrophy and abundant deposition of ECM in mice. These results suggested the successful construction of renal injury mouse model.

Radix Aucklandiae possesses the warm property and the function of pain relief and spleen strengthening.[32] As the main efficacy compounds in Radix Aucklandiae, CTD has many biological functions, including anti-inflammatory, antiulcer, and regulation of gastrointestinal function.[33] A recent study has shown that the development of renal fibrosis can be delayed or even reversed by CTD.[34] αSMA is a marker for myofibroblasts, and Collagen I and fibronectin are two of the most important ECM components.[35,36] Our findings suggest that treatment with CTD reduced the expression of αSMA, Collagen I, and Fibronectin in the kidneys of UUO-induced mice. Moreover, the UUO kidneys treated with CTD exhibited reduced intratubular space and decreased ECM deposition. These results indicate that CTD effectively improved renal function by blocking the development of renal fibrosis.

The present studies have revealed a strong association between inflammation and the progression of CKD.[37,38] Literatures have reported that the interaction of B and T lymphocytes can disturb the immune homeostasis and result in inflammation at different sites in CKD.[39] T lymphocyte-mediated cellular immunity is a major contributor to inflammation in the glomerulus and renal interstitium and can interact with DCs to aggravate renal tubular injury.[40] CD3 is a cell surface marker of T lymphocytes, which is associated with renal damage, as an indicator of the severity of kidney.[41] Previous report found that protein levels of TNF-α, NF-κB,
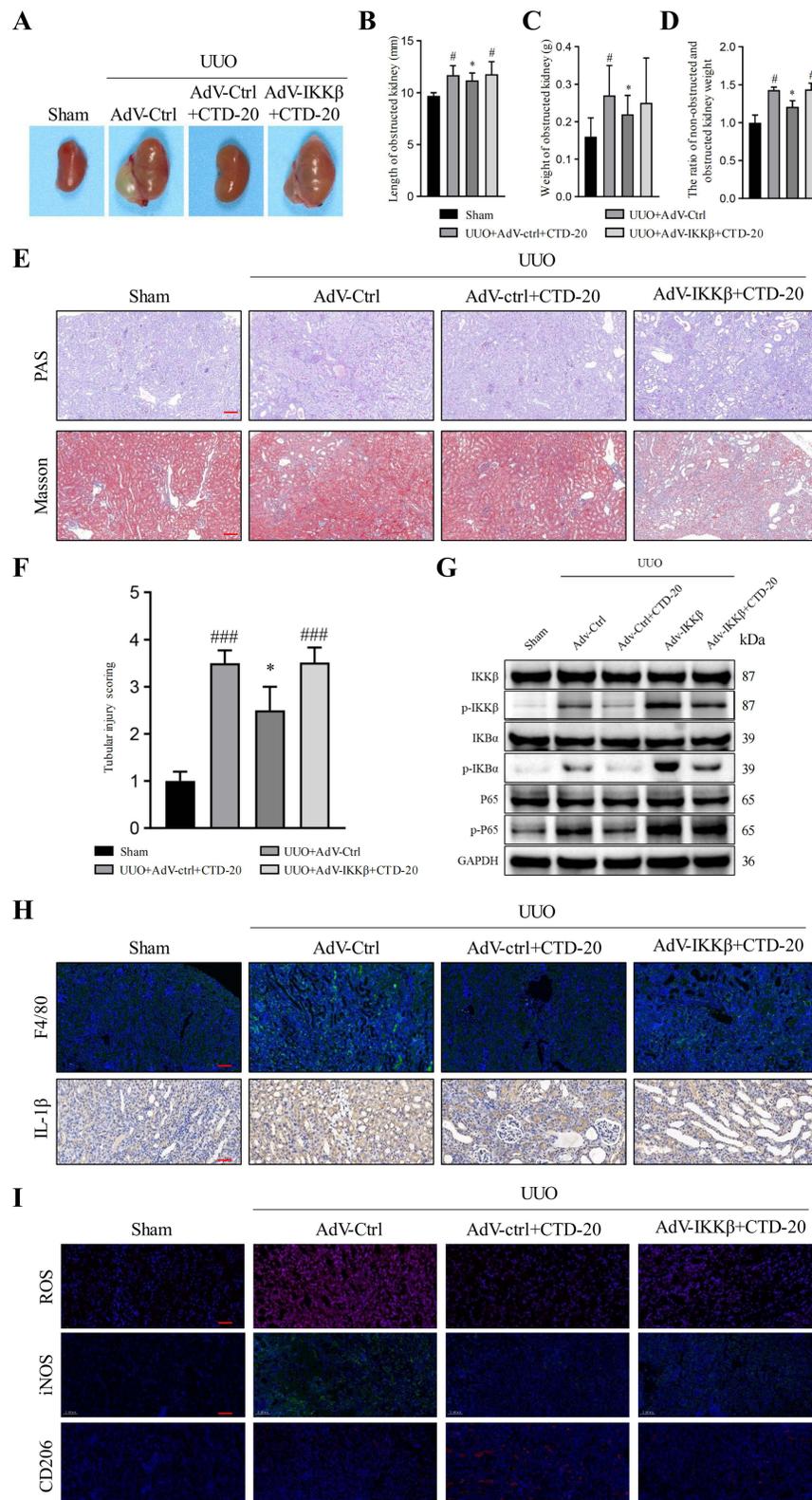
Figure 8 IKKβ overexpression partially attenuated the inhibitory effect of CTD on renal fibrosis in vivo. (**A**) Representative pictures of kidney of mice, (**B**) kidney length, (**C**) kidney weight, (**D**) the ratio of kidney weight to contralateral non-obstructed kidney weight of mice, (**E**) PAS and Masson staining of histological structure of kidney (×200 magnification), (**F**) tubular injury score of experimental mice, (**G**) Masson staining of kidneys in each group, (**G**) Western blot analysis of p-IKKβ, IKKβ, IκBα, p-IκBα, p-P65 and P65 in different groups, (**H**) immunofluorescence staining and IHC of F4/80 and IL-1β expression in kidneys. (**I**) representative pictures of ROS, iNOS, and CD206 staining of kidneys from different group. # $P < 0.05$, ### $P < 0.001$, compared to the sham group; *$P < 0.05$, compared to the UUO+AdV-ctrl+CTD-20 group, (n = 5 mice each group).

were reduced in serum of mice after CTD treatment.[42] Hence, we wonder whether CTD can alleviate renal injury by suppressing inflammatory response. Our results demonstrate that CLD treatment significantly decreased the expression of F4/80 (macrophages), Ly-6G (leukocytes), and CD3 (T cells). Additionally, our investigation detected decreased mRNA expression of inflammatory cytokines, such as TNF-α, Il-6, and Il-1β, in UUO kidneys treated with CTD. These findings indicate that CTD treatment can effectively reduce inflammation in CKD. Enhanced oxidative stress is a key factor in causing ferroptosis.[43] Although the mechanism by which ferroptosis affects CKD is unclear, ferroptosis affects kidney damage. In CKD, macrophages can produce proinflammatory cytokines and free radicals, which lead to lipid peroxidation and ferroptosis.[44] In addition, macrophages may also release lipid peroxidation products by engulfing dead cells, thereby affecting the survival of surrounding cells. However, in CKD, the macrophage antioxidant defense system is impaired, making it more susceptible to ferroptosis.[45] In our study, CTD treatment can significantly inhibit IKKβ-induced increase in Fe^{2+} content and lipid peroxidation levels in vivo and in vitro. CTD inhibits the occurrence of ferroptosis in THP-1 cell, which effectively improves the therapeutic effect of renal damage, providing new insights into clinical treatment. Our study demonstrated that CTD could polarize macrophages to M2 and alleviate macrophage ferroptosis induced by UUO or H_2O_2.

We performed RNA sequencing to further explore the molecular mechanisms of CTD attenuating renal injury. Enrichment analysis of KEGG pathways showed that NF-κB signaling pathways were the main pathways enriched in DEGs. This pathway is critical in regulating inflammation, making it an important target for study.[46] Various traditional Chinese medicines alleviate chronic renal injury and fibrosis levels by targeting the NF-κB signaling pathway. Fuzheng Huayu Formula can protect the kidney from HgCl2-induced oxidative damage by antagonizing NF-κB activity stimulated by oxidative stress, thereby alleviating the level of renal interstitial fibrosis.[47] Shenkang injection and its three anthraquinones (including chrysophanol, emodin, and rhein) alleviated the degree of renal damage in a rat model of chronic renal failure by inhibiting the expression of NF-κB (p65) protein.[48] Both icariin and geniposide can reduce the development of chronic kidney disease by regulating the NF-κB signaling pathway.[49,50] Considering that the NF-κB signaling pathway is a typical pro-inflammatory signaling pathway, targeting the NF-κB signaling pathway may be an effective way to treat CKD.

In the present study, IKKβ was used as the inflammation stimulator for the construction of cell inflammation model. The results of RT-qPCR and Western blot analyses were consistent with a previous report, indicating that IKKβ significantly increased the expression of inflammatory cytokines. However, CTD treatment significantly reduced the inflammation in mediated cell injury model. Inhibiting the expression of M1 macrophages or promoting the expression of M2 macrophages is one of the effective ways to treat renal fibrosis.[51,52] Therefore, macrophages play a key role in the pathogenesis of renal fibrosis, and our study shows that CTD can alleviate CKD by inhibiting the M1 macrophage marker (iNOS) and promoting the M2 macrophage marker (CD206). Within the macrophage population, M1 macrophages were defined as iNOS-positive and M2 macrophages as CD206-positive cells.[53] Macrophages of the M1 phenotype are pro-inflammatory, releasing inflammatory factors, while those of the M2 phenotype contributed to suppress inflammation.[54] In conclusion, these in vitro and in vivo experiments demonstrate that CTD attenuated renal injury by suppressing inflammation. We further investigated the effect of IKKβ on renal injury through AdV-mediated overexpression and siRNA interference. In vitro experiments showed that TNF-α expression in the medium was significantly decreased in the siRNA group and increased in the AdV-mRNA group, indicating that IKKβ can regulate the inflammatory process in cells. In vivo experiments further suggested that CTD may attenuate tubular injury, the deposition of ECM, and the inflammation to alleviate kidney damage by inhibiting IKKβ.

Conclusion

We suggest that CTD attenuated renal fibrosis and inflammation on renal damage through inhibiting IKKβ/NF-κB pathway, which provides a theoretical basis for clinical treatment for CKD (Figure 9).
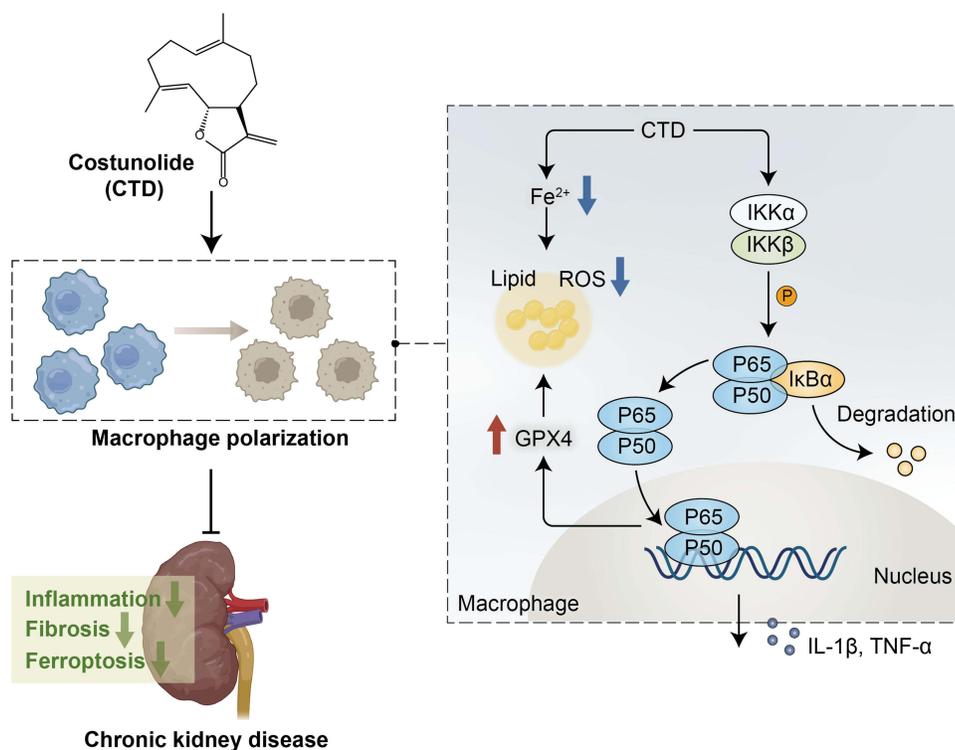
Figure 9 The mechanism of bioactive compound costunolide (CTD) on chronic kidney disease. Chronic kidney disease (CKD) is characterized by permanent changes in kidney structure and function. CTD alleviates renal injury by inhibiting oxidative stress, ferroptosis, inflammation and fibrosis. On the one hand, CTD can significantly inhibit the increase in Fe^{2+} content and IKKβ-induced lipid peroxidation levels. On the other hand, CTD alleviates inflammatory response by reducing the phosphorylation of IKKβ and P65, and affecting the polarization of macrophage toward M1 phenotype, (n = 5 mice each group).

Abbreviations

CKD, chronic kidney disease; CTD, costunolide; UUO, unilateral ureteral obstruction; AdV, adenovirus; HE, hematoxylin-eosin; PAS, periodic acid-Schiff; RT-qPCR, real-time quantitative PCR; ECM, extracellular matrix; MCP-1, monocyte chemoattractant protein 1; eGFR, estimated glomerular filtration rate; ROS, reactive oxygen species; GSH, glutathione; GPX4, glutathione peroxidase 4; AKI, acute kidney injury; IHC, immunohistochemistry; MDA, malondialdehyde; GSH, glutathione; SOD, superoxide dismutase; NF-κB, nuclear factor kappa B.

Data Sharing Statement

All data are provided in this study, and raw data can be requested from the corresponding author.

Ethics Approval and Consent to Participate

The authors are accountable for all aspects of the work in ensuring that questions related to the accuracy or integrity of any part of the work are appropriately investigated and resolved. The study was approved by Institutional Review Board of Shanghai Jiao Tong University School of Medicine Ruijin Hospital and Shanghai Jiao Tong University School of Medicine DLAS (Department of Laboratory Animal Science) No: RJ20230203.

Author Contributions

Mu-Jun Lu and Yuan Shao were the overall principal investigator who conceived the study, revised the manuscript and obtained financial support. Yang Zhao, Yi-Han Wang and Wei-Chao Tu performed the experiments and wrote the manuscript. Yang Zhao, Yi-Han Wang and Wei-Chao Tu collected the data and drew the figures and tables. Mu-Jun Lu, Da-Wei Wang and Yuan Shao reviewed the manuscript critically. Yang Zhao and Yi-Han Wang contributed equally to this work and should be regarded as co-first authors. All authors made a significant

contribution to the work reported, whether that is in the conception, study design, execution, acquisition of data, analysis and interpretation, or in all these areas; took part in drafting, revising or critically reviewing the article; gave final approval of the version to be published; have agreed on the journal to which the article has been submitted; and agree to be accountable for all aspects of the work.

Funding

Disclosure

The authors report no conflicts of interest in this work.

References

1. Kidney Disease: Improving Global Outcomes (KDIGO) Diabetes Work Group. KDIGO 2020 clinical practice guideline for diabetes management in chronic kidney disease. *Kidney Int*. 2020;98(4S):S1–S115. doi:10.1016/j.kint.2020.06.019
2. Ammirati AL. Chronic Kidney Disease. *Rev Assoc Med Bras*. 2020;66(Suppl 1):s03–s09. doi:10.1590/1806-9282.66.S1.3
3. Jha V, Garcia-Garcia G, Iseki K, et al. Chronic kidney disease: global dimension and perspectives. *Lancet*. 2013;382(9888):260–272. doi:10.1016/S0140-6736(13)60687-X
4. Wu P-H, Lin Y-T, Chiu Y-W, et al. The relationship of indoxyl sulfate and P-cresyl sulfate with target cardiovascular proteins in hemodialysis patients. *Sci Rep*. 2021;11(1):3786. doi:10.1038/s41598-021-83383-x
5. Dong Z, Sun Y, Wei G, Li S, Zhao Z. A nucleoside/nucleobase-rich extract from cordyceps sinensis inhibits the epithelial–mesenchymal transition and protects against renal fibrosis in diabetic nephropathy. *Molecules*. 2019;24(22):4119. doi:10.3390/molecules24224119
6. You Y-K, Luo Q, Wu W-F, et al. Petchiether A attenuates obstructive nephropathy by suppressing TGF-β/Smad3 and NF-κB signalling. *J Cell & Mol Med*. 2019;23(8):5576–5587. doi:10.1111/jcmm.14454
7. Zhang X, Ritter JK, Li N. Sphingosine-1-phosphate pathway in renal fibrosis. *Am J Physiol Renal Physiol*. 2018;315(4):F752–F756. doi:10.1152/ajprenal.00596.2017
8. Ren L, Guo X-Y, Gao F, Jin M-L, Song X-N. Identification of the perturbed metabolic pathways associating with renal fibrosis and evaluating metabolome changes of pretreatment with astragalus polysaccharide through liquid chromatography quadrupole time-of-flight mass spectrometry. *Front Pharmacol*. 2020;10:1623. doi:10.3389/fphar.2019.01623
9. Kim S, Kang S-W, Joo J, et al. Characterization of ferroptosis in kidney tubular cell death under diabetic conditions. *Cell Death Dis*. 2021;12(1):1–14. doi:10.1038/s41419-021-03452-x
10. Zhang S, Wu J, Wang H, et al. Liposomal oxymatrine in hepatic fibrosis treatment: formulation. *Asse AAPS Pharm*. 2014;15(3):620–629. doi:10.1208/s12249-014-0086-y
11. Kadatane SP, Satariano M, Massey M, Mongan K, Raina R. The Role of Inflammation in CKD. *Cells*. 2023;12(1581):1581. doi:10.3390/cells12121581
12. Mihai S, Codrici E, Popescu ID, et al. Inflammation-related mechanisms in chronic kidney disease prediction, progression, and outcome. *J Immunol Res*. 2018;2018:2180373. doi:10.1155/2018/2180373
13. Agharazii M, St-Louis R, Gautier-Bastien A, et al. Inflammatory cytokines and reactive oxygen species as mediators of chronic kidney disease-related vascular calcification. *Am J Hypertens*. 2015;28(6):746–755. doi:10.1093/ajh/hpu225
14. Luan J, Fu J, Jiao C, et al. IL-18 deficiency ameliorates the progression from AKI to CKD. *Cell Death Dis*. 2022;13(11):957. doi:10.1038/s41419-022-05394-4
15. Ma L-J, Corsa BA, Zhou J, et al. Angiotensin Type 1 Receptor Modulates Macrophage Polarization and Renal Injury in Obesity. *Am J Physiol Renal Physiol*. 2011;300(5):F1203–1213. doi:10.1152/ajprenal.00468.2010
16. Tseng K-F, Tsai P-H, Wang J-S, Chen F-Y, Shen M-Y. Sesamol attenuates renal inflammation and arrests reactive-oxygen-species-mediated IL-1β secretion via the HO-1-induced inhibition of the ikkα/nfkb pathway in vivo and in vitro. *Antioxidants*. 2022;11(12):2461. doi:10.3390/antiox11122461
17. Li J, Cao F, Yin H-L, et al. Ferroptosis: past, present and future. *Cell Death Dis*. 2020;11(2):88. doi:10.1038/s41419-020-2298-2
18. Yang WS, Stockwell BR. Synthetic lethal screening identifies compounds activating iron-dependent, nonapoptotic cell death in oncogenic-RAS-harboring cancer cells. *Chem Biol*. 2008;15(3):234–245. doi:10.1016/j.chembiol.2008.02.010
19. Takada Y, Itoh H, Paudel A, et al. Discovery of gramicidin a analogues with altered activities by multidimensional screening of a one-bead-one-compound library. *Nat Commun*. 2020;11(1):4935. doi:10.1038/s41467-020-18711-2
20. Rasul A, Bao R, Malhi M, et al. Induction of apoptosis by costunolide in bladder cancer cells is mediated through ROS generation and mitochondrial dysfunction. *Molecules*. 2013;18(2):1418–1433. doi:10.3390/molecules18021418
21. Wei M, Li J, Qiu J, et al. Costunolide induces apoptosis and inhibits migration and invasion in H1299 lung cancer cells. *Oncol Rep*. 2020;43(6):1986–1994. doi:10.3892/or.2020.7566
22. Hu M, Liu L, Yao W. Activation of P53 by costunolide blocks glutaminolysis and inhibits proliferation in human colorectal cancer cells. *Gene*. 2018;678:261–269. doi:10.1016/j.gene.2018.08.048
23. Zhuge W, Chen R, Vladimir K, et al. Costunolide specifically binds and inhibits thioredoxin reductase 1 to induce apoptosis in colon cancer. *Cancer Lett*. 2018;412:46–58. doi:10.1016/j.canlet.2017.10.006
24. Inan MS, Razzaque MS, Taguchi T. Pathological significance of renal expression of NF-kappa B. *Contrib Nephrol*. 2003;139:90–101. doi:10.1159/000071738

25. Ren N, Wang W-F, Zou L, Zhao Y-L, Miao H, Zhao -Y-Y. The nuclear factor kappa b signaling pathway is a master regulator of renal fibrosis. *Front Pharmacol*. 2023;14:1335094. doi:10.3389/fphar.2023.1335094

26. He Y, Moqbel SAA, Xu L, et al. Costunolide inhibits matrix metalloproteinases expression and osteoarthritis via the NF-κB and Wnt/B-catenin signaling pathways. *Mol Med Rep*. 2019;20(1):312–322. doi:10.3892/mmr.2019.10239

27. Liu B, Rong Y, Sun D, et al. Costunolide inhibits pulmonary fibrosis via regulating NF-kB and TGF-B1/Smad2/Nrf2-NOX4 signaling pathways. *Biochem Biophys Res Commun*. 2019;510(2):329–333. doi:10.1016/j.bbrc.2019.01.104

28. Ren Y, Du C, Yan L, et al. CTGF siRNA ameliorates tubular cell apoptosis and tubulointerstitial fibrosis in obstructed mouse kidneys in a sirt1-independent manner. *Drug Des Devel Ther*. 2015;9:4155–4171. doi:10.2147/DDDT.S86748

29. Zhang Q-F. Ulinastatin inhibits renal tubular epithelial apoptosis and interstitial fibrosis in rats with unilateral ureteral obstruction. *Mol Med Rep*. 2017;16(6):8916–8922. doi:10.3892/mmr.2017.7692

30. Kang D-H, Nakagawa T, Feng L, Johnson RJ. Nitric oxide modulates vascular disease in the remnant kidney model. *Am J Pathol*. 2002;161 (1):239–248. doi:10.1016/S0002-9440(10)64175-2

31. Yang R, Xu X, Li H, et al. P53 Induces miR199a-3p to Suppress SOCS7 for STAT3 activation and renal fibrosis in UUO. *Sci Rep*. 2017;7(1):43409. doi:10.1038/srep43409

32. Li J, Bai L, Wei F, et al. Therapeutic mechanisms of herbal medicines against insulin resistance: a review. *Front Pharmacol*. 2019;10:661. doi:10.3389/fphar.2019.00661

33. Zheng H, Chen Y, Zhang J, et al. Evaluation of protective effects of costunolide and dehydrocostuslactone on ethanol-induced gastric ulcer in mice based on multi-pathway regulation. *Chem Biol Interact*. 2016;250:68–77. doi:10.1016/j.cbi.2016.03.003

34. Fu D, Wu D, Cheng W, et al. Costunolide induces autophagy and apoptosis by activating ROS/MAPK signaling pathways in renal cell carcinoma. *Front Oncol*. 2020;10:582273. doi:10.3389/fonc.2020.582273

35. Yan Q, Luo H, Wang B, et al. Correlation between PKB/Akt, GSK-3β expression and tubular epithelial-mesenchymal transition in renal allografts with chronic active antibody-mediated rejection. *Exp Ther Med*. 2017;13(5):2217–2224. doi:10.3892/etm.2017.4261

36. Xing Q, Yates K, Tahtinen M, Shearier E, Qian Z, Zhao F. Decellularization of fibroblast cell sheets for natural extracellular matrix scaffold preparation. *Tissue Eng Part C Methods*. 2015;21(1):77–87. doi:10.1089/ten.tec.2013.0666

37. Aoki K, Teshima Y, Kondo H, et al. Role of indoxyl sulfate as a predisposing factor for atrial fibrillation in renal dysfunction. *J Am Heart Assoc*. 2015;4(10):e002023. doi:10.1161/JAHA.115.002023

38. Chambers SM, Boles NC, Lin K-YK, et al. Hematopoietic fingerprints: an expression database of stem cells and their progeny. *Cell Stem Cell*. 2007;1(5):578–591. doi:10.1016/j.stem.2007.10.003

39. Panzer U, Kurts C. T cell cross-talk with kidney dendritic cells in glomerulonephritis. *J Mol Med*. 2010;88(1):19–26. doi:10.1007/s00109-009-0541-5

40. Sood P, Hariharan S. Anti-CD20 Blocker Rituximab in Kidney Transplantation. *Transplantation*. 2018;102(1):44–58. doi:10.1097/TP.0000000000001849

41. Wang J, Huang L, Mou C, et al. Mucosal immune responses induced by oral administration recombinant Bacillus subtilis expressing the COE antigen of PEDV in newborn piglets. *Biosci Rep*. 2019;39(3):BSR20182028. doi:10.1042/BSR20182028

42. Xie F, Zhang H, Zheng C, Shen X-F. Costunolide improved dextran sulfate sodium-induced acute ulcerative colitis in mice through NF-κB, STAT1/3, and Akt signaling pathways. *Int Immunopharmacol*. 2020;84:106567. doi:10.1016/j.intimp.2020.106567

43. Zhou B, Zhang J-Y, Liu X-S, et al. Tom20 senses iron-activated ROS signaling to promote melanoma cell pyroptosis. *Cell Res*. 2018;28 (12):1171–1185. doi:10.1038/s41422-018-0090-y

44. Zhang Y, Zhang Z, Huang L, et al. Augmenter of liver regeneration knockout aggravates tubular ferroptosis and macrophage activation by regulating carnitine palmitoyltransferase-1A-induced lipid metabolism in diabetic nephropathy. *Acta Physiol*. 2024;2024:e14159. doi:10.1111/apha.14159

45. Wang Y, Shen Z, Mo S, et al. Crosstalk among proximal tubular cells, macrophages, and fibroblasts in acute kidney injury: single-cell profiling from the perspective of ferroptosis. *Hum Cell*. 2024;37(4):1039–1055. doi:10.1007/s13577-024-01072-z

46. An G, Wu F, Huang S, et al. Effects of CCL5 on the biological behavior of breast cancer and the mechanisms of its interaction with tumor-associated macrophages. *Oncol Rep*. 2019;42(6):2499–2511. doi:10.3892/or.2019.7344

47. Yuan J-L, Tao -Y-Y, Wang Q-L, Shen L, Liu C-H. Fuzheng huayu formula () prevents rat renal interstitial fibrosis induced by HgCl2 via antioxidative stress and down-regulation of nuclear factor-kappa b activity. *Chin J Integr Med*. 2017;23(8):598–604. doi:10.1007/s11655-016-2540-z

48. Luo L-P, Suo P, Ren -L-L, Liu H-J, Zhang Y, Zhao -Y-Y. Shenkang injection and its three anthraquinones ameliorates renal fibrosis by simultaneous targeting IκB/NF-κB and Keap1/Nrf2 signaling pathways. *Front Pharmacol*. 2021;12:800522. doi:10.3389/fphar.2021.800522

49. Zhang L, Wang X-Z, Li Y-S, Zhang L, Hao L-R. Icariin ameliorates IgA nephropathy by inhibition of nuclear factor kappa b/Nlrp3 Pathway. *FEBS Open Bio*. 2017;7(1):54–63. doi:10.1002/2211-5463.12161

50. Hu X, Zhang X, Jin G, Shi Z, Sun W, Chen F. Geniposide reduces development of streptozotocin-induced diabetic nephropathy via regulating nuclear factor-Kappa B signaling pathways. *Fundam Clin Pharmacol*. 2017;31(1):54–63. doi:10.1111/fcp.12231

51. Chen J, Tang Y, Zhong Y, et al. P2Y12 inhibitor clopidogrel inhibits renal fibrosis by blocking macrophage-to-myofibroblast transition. *Mol Ther*. 2022;30(9):3017–3033. doi:10.1016/j.ymthe.2022.06.019

52. Chen M, Menon MC, Wang W, et al. HCK induces macrophage activation to promote renal inflammation and fibrosis via suppression of autophagy. *Nat Commun*. 2023;14(1):4297. doi:10.1038/s41467-023-40086-3

53. Antonios JK, Yao Z, Li C, Rao AJ, Goodman SB. Macrophage polarization in response to wear particles in vitro. *Cell Mol Immunol*. 2013;10 (6):471–482. doi:10.1038/cmi.2013.39

54. Tong WW, Zhang C, Hong T, et al. Silibinin alleviates inflammation and induces apoptosis in human rheumatoid arthritis fibroblast-like synoviocytes and has a therapeutic effect on arthritis in rats. *Sci Rep*. 2018;8(1):3241. (). doi:10.1038/s41598-018-21674-6